

# X-ray Absorption Near-Edge Structure calculations with pseudopotentials.

## Application to K-edge in diamond and $\alpha$ -quartz

Mathieu Taillefumier<sup>1</sup>, Delphine Cabaret<sup>1</sup>, Anne-Marie Flank<sup>2</sup>, Francesco Mauri<sup>1</sup>

<sup>1</sup> Laboratoire de Minéralogie-Cristallographie de Paris,  
Université Pierre et Marie Curie, case 115,  
4 place Jussieu, 75252 Paris cedex 05, France

<sup>2</sup> Laboratoire pour l'Utilisation du Rayonnement Electromagnetique,  
Centre universitaire Paris-sud, Bât. 209D, 91898 Orsay cedex, France

### Abstract

We present a reciprocal-space pseudopotential scheme for calculating X-ray absorption near-edge structure (XANES) spectra. The scheme incorporates a recursive method to compute absorption cross section as a continued fraction. The continued fraction formulation of absorption is advantageous in that it permits the treatment of core-hole interaction through large supercells (hundreds of atoms). The method is compared with recently developed Bethe-Salpeter approach. The method is applied to the carbon K-edge in diamond and to the silicon and oxygen K-edges in  $\alpha$ -quartz for which polarized XANES spectra were measured. Core-hole effects are investigated by varying the size of the supercell, thus leading to information similar to that obtained from cluster size analysis usually performed within multiple scattering calculations.

## 1 Introduction

XANES spectroscopy is a powerful technique to probe the empty states in solids. Moreover XANES gives information about the atomic arrangement around the probed atom up to the medium range order (i.e., about 8 Å). Nevertheless the interpretation of XANES spectra is not straightforward and often requires sophisticated simulation tools. To calculate a XANES spectrum, one needs to compute the absorption cross section. This is given by the Fermi golden rule as a sum of probabilities per unit of time of making a transition from an initial state to an unoccupied final state through an interaction Hamiltonian [1]. Electronic transitions involved in X-ray absorption spectroscopy are mainly governed by the electric dipole operator. The main difficulty of any absorption cross section calculation lies in the solution of the Schrödinger equation for the final and initial states. The choice of the method used to solve the Schrödinger equation depends on the localized or delocalized character of final states. Crystal field multiplet theory [2] is adapted to the calculation of localized final states, i.e., with strong electron-electron interactions. It is typically the case of  $L_{2,3}$  edges of transition elements [3] and  $M_{4,5}$  edges of rare earth elements [4]. If the final state is delocalized (the case of K and  $L_1$  edges) multielectronic interactions are weak and mono-electronic approaches based on the density functional theory (DFT) are usually employed. Among mono-electronic methods, one distinguishes the real space (cluster) approach from the reciprocal space (band structure) approach. Real space multiple scattering theory [5, 6, 7] has been extensively used in the past twenty years. However, multiple scattering theory suffers from an unavoidable drawback, i.e., the "muffin-tin" approximation of the potential. Recently, the "muffin-tin" approximation has been overtaken in a real space approach by using the finite difference method (MDF) to solve the Schrödinger equation [8]. Although it yields good results [9], the method presented in Ref. [8] requires significant computing power. At present this is what restricts the applications to small clusters (around 50 atoms without any symmetry, at maximum).

With regards to band structure calculations, local projected densities of empty states (commonly called LDOS) have been often used to interpret XANES spectra (see for instance Refs. [10, 11, 12]). Recently several band structure codes have incorporated the radial matrix elements [13] to properly

calculate XANES or ELNES (electron energy-loss near-edge structure). It is notably the case of Wien2k [14], which is based on the full-potential linearized augmented plane wave method [15], the orthogonalized-linear-combination-of-atomic-orbital program developed by Mo and Ching [16, 17] and CASTEP, whose ELNES part has been developed by Pickard [18, 19, 20]. This last approach uses pseudopotentials and reconstructs all electron wave functions within the projector augmented wave (PAW) method of Blochl [21]. Within these ab initio schemes the treatment of core-hole-electron interactions is usually achieved through the inclusion of an excited atom into a supercell. The absorbing atom is then considered as an impurity. Beside these methods, Shirley [22] and more recently Soininen and Shirley [23] have proposed alternative formalisms that treat core-hole interactions in a different way. Indeed their methods incorporate core-hole interactions in the two-particle Bethe-Salpeter (BS) equation. Such methods are of great importance for optical absorption calculations [24, 25, 26, 27]. However, in the case of K-edge XANES spectra, the core-hole is frozen at one atomic site and the two-particle BS approach can be reduced to a single particle calculation.

By using supercell approaches, large systems (several hundreds of atoms) can be a priori treated. The charge density for such large cells is easy to calculate self-consistently by using pseudopotentials. On the other hand, the computation of the cross section is at present limited by the diagonalisation of the Hamiltonian for several empty states at many k-points in the Brillouin zone. Indeed in Refs. [18, 19] pseudopotential calculations of ELNES spectra in diamond and c-BN have been performed with a small 16-atom supercell. Here we propose to use the recursion method of Haydock, Heine and Kelly [30, 31, 28] to make the calculation of the cross section computationally tractable for larger supercells. Thanks to this iterative technique, the calculation time of XANES becomes negligible compared with the calculation of the self-consistent charge density in large systems.

We incorporated the recursion method into a pseudopotential scheme. We first show in section 2 that the absorption cross section can be easily computed within a pseudopotential formalism using the PAW method. Then, by using the recursion method, we express the absorption cross section as a continued fraction. We present applications to K-edges in section 3. Two materials have been chosen : diamond which is an interesting example for method testing, and  $\alpha$ -quartz for which we have measured polarized XANES spectra.

## 2 Method

### 2.1 X-ray absorption cross section in the impurity model

In a mono-electronic approach, the X-ray absorption cross section  $\sigma(\omega)$  can be written as

$$\sigma(\omega) = 4\pi^2 \omega^{-2} \sum_{f \neq i}^X |M_{if}|^2 \delta(E_f - E_i - \omega); \quad (1)$$

where  $\omega$  is the photon energy,  $\omega_0$  is the fine structure constant and  $M_{if}$  are the transition amplitudes between an initial core state  $j_i$  with energy  $E_i$ , localized on the absorbing atom site  $R_0$ , and an allelectronnal state  $j_f$  with energy  $E_f$

$$M_{if} = \langle j_f | \hat{O} | j_i \rangle \quad (2)$$

$\hat{O}$  is a transition operator coupling initial and final states. In the electric quadrupole approximation,  $\hat{O}$  is given by  $\epsilon_{ijk} r_i (1 + \frac{1}{2} k_j r_k)$ , where  $\epsilon$  and  $k$  are the polarisation vector and the wave vector of the photon beam, respectively. Within the frozen core approximation,  $j_i$  is a core state that can be taken from an allelectron ground state atomic calculation. In the impurity model,  $j_f$  is an excited empty state that is solution of the Schrodinger equation for a potential that includes a core-hole on the absorbing atom.

### 2.2 PAW formalism

In the following we want to express the transition amplitude (Eq.2) within the PAW formalism, as originally described by Blochl [21]. We only recall the main aspects of the method that are needed to give a simple expression for the  $M_{if}$  terms.

Within the PAW formalism, the final state allelectron wave functions  $j_f$  are related to the corresponding final pseudo wave functions  $j_f^p$  through a linear operator  $T$ :

$$j_f = T j_f^p \quad (3)$$

T differs from identity by a sum of local atom-centered contributions, that act only within spherical core regions centered on each atomic site  $R$ , called augmentation regions or  $\mathcal{R}$ :

$$T = 1 + \sum_{R,n} h_{R,n}^i j_{R,n}^i - j_{R,n}^e i h_{R,n}^j \quad (4)$$

Here  $j_{R,n}^i$  and  $j_{R,n}^e$  are the all electron and pseudo partial waves, respectively, which coincide outside  $\mathcal{R}$ . The vectors  $h_{R,n}^j$  called projector functions [21], are equal to zero outside  $\mathcal{R}$  and satisfy the condition  $h_{R,n}^j j_{R_0,n_0}^i = \delta_{R,R_0} \delta_{n,n_0}$ . The index  $n$  refers to the angular momentum quantum numbers ( $l, m$ ) and to an additional number, used if there is more than one projector per angular momentum channel. The  $j_{R,n}^i$  form a complete basis for any physical non-core all electron wave function within  $\mathcal{R}$  [29]. Therefore the  $j_{R,n}^e$  are also a complete basis for any physical pseudo wave function  $j^e$  within  $\mathcal{R}$ , i.e. for any  $h_{R,n}^j$  function centered on an atomic site  $R$  and equal to zero outside  $\mathcal{R}$ ,

$$\sum_n h_{R,n}^j i h_{R,n}^e j_{R,n}^i = h_{R,n}^j i \quad (5)$$

Substituting Eq. (4) in Eq. (3) and then Eq. (3) in Eq. (2), the transition amplitude  $M_{i \rightarrow f}$  becomes

$$M_{i \rightarrow f} = h_{f,i}^e j_{i,i}^i + \sum_{R,n} h_{R,n}^e i h_{R,n}^j j_{i,i}^i + \sum_{R,n} h_{R,n}^e i h_{R,n}^e j_{i,i}^i \quad (6)$$

In Eq.6, the initial wave function  $h_{i,i}^j$  is localized on the site of the absorbing atom,  $R_0$ , then only the  $R_0$  term has to be considered in each sum. Furthermore it should be noticed that  $h_{i,i}^j$  is zero outside the  $\mathcal{R}_{R_0}$  region. Therefore we can make use of Eq.(5) for the third term of Eq.(6), which thus vanishes with the first term. The transition amplitude  $M_{i \rightarrow f}$  is then reduced to one term. Now, introducing

$$j_{R_0,n}^e i = \sum_n j_{R_0,n}^e i h_{R_0,n}^j j_{i,i}^i; \quad (7)$$

we obtain the following simple expression for the X-ray absorption cross section

$$\sigma_f = 4 \pi^2 \sum_f | \sum_i h_{f,i}^e j_{R_0,n}^e i |^2 (E_f - E_i \sim \epsilon): \quad (8)$$

The calculation of XANES spectra from Eq.8 presents us with the problem of determining many empty states  $j_{f,i}^e$ , as has been mentioned in section 1. Indeed, the addition of unoccupied bands significantly increases computing time and then limits the size of the supercells. In the following, we show how the recursion method permits the cross section (Eq.8) to be rewritten as a continued fraction, so that only occupied bands have to be calculated.

## 2.3 Recursion method

The recursion method comprises of a powerful recursive algorithm that can be applied to a Hermitian matrix in order to transform it into a tridiagonal form. This method has been widely used in solid states physics. The pioneering works in this field were mainly by Haydock, Heine and Kelly [30, 31]. The first application to absorption cross section calculation was carried out by Filipponi within the multiple scattering formalism [32]. In a close field Benedict and Shirley have implemented it for  $\sigma_2(\epsilon)$  calculation including core-hole interaction [33] within the BS approach. For simplicity, in the following, we assume that the norm of all electron partial waves coincide with that of the pseudo-partial waves.

In order to use the recursion method in our scheme, we shall introduce the Green operator into Eq.(8) by making the substitution

$$j_{f,i}^e (E_f - E_i \sim \epsilon) h_{f,i}^e j = \frac{1}{-i\epsilon - \mathcal{G}(E)}; \quad (9)$$

with

$$\mathcal{G}(E) = (E - \mathbb{H} + i)^{-1} \quad (10)$$

In Eq.(10)  $\mathcal{G}(E)$  is the Green operator associated with the pseudo-Hamiltonian  $\mathbb{H} = T^{\dagger} H T$ , which is Hermitian. The energy  $E$  is given by  $E = E_i + i\eta$  and  $\eta$  is an infinitesimal positive number. The cross section (Eq.8) can be rewritten as

$$\sigma_i = 4\pi\eta \text{Im} \langle \mathbf{e}_{R_0} | \mathcal{G}(E - \mathbb{H} + i)^{-1} | \mathbf{e}_{R_0} \rangle \quad (11)$$

Following the original work of Lanczos [34, 35], the recursion method sets up a new basis in which the pseudo-Hamiltonian  $\mathbb{H}$ , has a tridiagonal representation, from which the matrix elements  $\langle \mathbf{e}_{R_0} | \mathcal{G}(E - \mathbb{H} + i)^{-1} | \mathbf{e}_{R_0} \rangle$  are very simply derived. This new basis (called Lanczos basis in the following) is obtained by the repeated action of  $\mathbb{H}$  onto the normalized initial vector  $|\mathbf{e}_{R_0}\rangle = \mathbb{H} |\mathbf{e}_{R_0}\rangle / \langle \mathbf{e}_{R_0} | \mathbb{H}^2 | \mathbf{e}_{R_0} \rangle^{1/2}$  through the symmetric three-term recurrence relation

$$\mathbb{H} |\mathbf{e}_{i+1}\rangle = a_{i+1} |\mathbf{e}_{i+1}\rangle + b_{i+1} |\mathbf{e}_{i+2}\rangle + b_i |\mathbf{e}_i\rangle \quad (12)$$

where  $a_i$  and  $b_i$  are two sets of real parameters given by  $a_i = \langle \mathbf{e}_i | \mathbb{H} | \mathbf{e}_i \rangle$  and  $b_i = \langle \mathbf{e}_i | \mathbb{H} | \mathbf{e}_{i+1} \rangle = \langle \mathbf{e}_{i+1} | \mathbb{H} | \mathbf{e}_i \rangle$ . The tridiagonal matrix representation of  $\mathbb{H}$  in the  $|\mathbf{e}_i\rangle$  basis then leads to the following form of the matrix elements of Eq. (11)

$$\langle \mathbf{e}_{R_0} | \mathcal{G}(E - \mathbb{H} + i)^{-1} | \mathbf{e}_{R_0} \rangle = \frac{\langle \mathbf{e}_{R_0} | \mathbb{H} | \mathbf{e}_{R_0} \rangle}{a_0 - E - \frac{b_1^2}{a_1 - E - \frac{b_2^2}{\ddots}}} \quad (13)$$

A simple terminator has been used to finish the continued fraction [33]. In particular, if  $N$  is the number of iterations required to converge the calculation, we consider that the coefficients  $(a_i; b_i)$  are equal to  $(a_N; b_N)$  for  $i > N$ , this leads to an analytical form of the terminator. It should be noted that the number of iterations  $N$  strongly depends on the broadening parameter  $\eta$ . With the iterative technique of Haydock the main part of XANES calculation involves the computation of the Hamiltonian acting on a single vector. This means that the computing time is considerably reduced compared to that can be required by Eq. 8 with an explicit diagonalisation.

## 2.4 Comparison with Bethe-Salpeter approach

Recently, the BS approach has been successfully applied to the calculation of XANES [22, 23]. Since the formalism of such two particles excited states calculations has been recently detailed in a review [36], here we only recall the main aspects. The BS procedure [23] consists of a ground state DFT calculation in order to obtain the Kohn-Sham orbitals, a GW calculation to correct the eigenvalues [37], and a solution of BS equation using GW eigenvalues and a statically screened potential.

Our method differs from the BS approach of Soininen and Shirley [23] by three points. The first two differences are substantial, the last one is just methodological. In particular, (i) we use the DFT eigenvalues, whereas Ref. [23] uses GW corrected eigenvalues [37]. If the GW correction on the empty states can be described by a rigid shift, as it is often the case, this difference will not affect the XANES spectra. (ii) We screen the core-hole by the valence electron response at all orders computed self-consistently within DFT. In Ref. [23], the core-hole is screened at the linear order using the random phase approximation [38]. (iii) We develop the final state wave functions  $|\mathbf{f}_f\rangle$  in a plane wave basis set of a supercell. In Ref. [23], the BS calculation uses as basis the eigenstates of the ground state Hamiltonian.

In the next section, our results will be compared with BS calculations as far as possible.

## 3 Applications

Our method was applied to the carbon K-edge in the diamond phase and to the silicon and oxygen K-edges in  $\alpha$ -quartz. XANES calculations were performed in two steps: (i) the evaluation of the self-consistent charge density for supercells including one 1s core-hole, (ii) the construction of a converged  $|\mathbf{e}_i\rangle$  basis leading to the tridiagonal representation of the pseudo-Hamiltonian. The transition matrix elements were determined in the electric dipole approximation. Calculations were carried out using an ab initio total energy code based on density functional theory within the local density approximation (LDA) [39]. Norm-conserving Troullier-Martins pseudopotentials [40] with a

single component for each ( $\pi$ ) component were used. For the excited atom a pseudopotential with only one 1s electron was generated. In both diamond and  $\alpha$ -quartz cases, the size of the supercell was increased until the neighboring excited potentials did not interact with each other. The wave functions were expanded in plane waves with an energy cutoff of 50 Ry and 70 Ry for diamond and  $\alpha$ -quartz respectively. Reciprocal-space integrations were performed using a Monkhorst-Pack k-point grid [41].

### 3.1 Diamond

Figure 1 shows calculations performed with four different sizes of supercell, all including a 1s core-hole on one of the carbon atoms. The size of the primitive cell (trigonal cell ( $a = 2.524 \text{ \AA}$ ) containing two carbon atoms) was successively multiplied in the three directions by a factor two ( $2 \times 2 \times 2$  supercell, 16 atoms), three ( $3 \times 3 \times 3$  supercell, 54 atoms), four ( $4 \times 4 \times 4$  supercell, 128 atoms) and five ( $5 \times 5 \times 5$  supercell, 250 atoms). Further increasing the supercell size does not provide significant modifications in the calculated spectrum. k-point convergence of the charge density was obtained with a  $2 \times 2 \times 2$  k-point grid for both  $2 \times 2 \times 2$  and  $3 \times 3 \times 3$  supercells, and with only one k-point for larger supercells. k-point convergence of the Lanczos basis was reached with a  $10 \times 10 \times 10$  k-point grid for the  $2 \times 2 \times 2$  supercell, a  $8 \times 8 \times 8$  k-point grid for the  $3 \times 3 \times 3$  supercell, and  $6 \times 6 \times 6$  k-point grids for both  $4 \times 4 \times 4$  and  $5 \times 5 \times 5$  supercells. The number of iterations of the Lanczos basis was checked with  $\epsilon = 0.3 \text{ eV}$ . The required number of jui vectors varied from around 800 to 1400, while increasing the supercell size from 16 atoms to 250 atoms.

Calculations are compared with the carbon K-XANES spectrum of diamond measured by Ma et al. [42]. The overall agreement between the experimental spectrum and the  $5 \times 5 \times 5$  supercell calculated one is quite good. In particular, the features from d to i are correctly reproduced as well in relative intensity as in energy position. Nevertheless in the first four eV of the spectrum the agreement between experiment and calculation remains unsatisfactory. The intensity of peak b is exaggerated and the exciton peak a is not reproduced. Looking at the various supercell calculations, one notices that the first 25 eV of the spectrum are affected by the size of the cell, i.e. the interaction between core-holes belonging to neighboring cells. This gives information about the volume seen by the photoelectron during the absorption process: the photoelectron interacts with atoms located within a 6 Å radius sphere centered on the absorbing atom.

Several calculations of the carbon K-edge in diamond have been reported in the literature. Weng et al. [43] present pseudo-atomic-orbital density of empty states together with multiple scattering calculations. On the one hand,  $\mu$ -n-tin" potentials as required in multiple scattering theory appear to be inappropriate in that case. This result was confirmed by a 300 atom cluster calculation performed by the FEFF8 code [7, 44]. On the other hand, although it neglects core-hole effects, LDOS calculation by Weng et al. [43] seems to correctly reproduce features h and i. Pickard [18] shows that including core-hole effects into a  $2 \times 2 \times 2$  supercell significantly improves the agreement with experiment. However, as the supercell size increases, peak b becomes much too intense (Figure 1). This may suggest an overestimation of the core-hole effects in that case. This result has also been observed by Soininen and Shirley [23] while core-hole interactions is treated within BS approach. Their carbon K edge calculation in diamond, is however very similar to our 128 and 250 atom supercell spectra. It seems that the corrections brought to excited states by GW calculations has only a negligible influence on the energy positions of calculated features. This result is not surprising since previous studies [45, 46] have shown that the GW approximation used for band structure calculation in diamond, amounts to applying a scissors-operator shift which is valid to within a 0.5 eV error. This error is comparable to the energy resolution of XANES features. The exaggeration of peak b in both calculations requires more understanding and the problem of the treatment of core-hole interaction in diamond is at this time still unclear.

### 3.2 $\alpha$ -quartz

In the case of  $\alpha$ -quartz, calculations are compared with polarized Si and O K-XANES experiments.  $\alpha$ -quartz ( $\text{SiO}_2$ ) has a trigonal space group with a hexagonal unit cell. Since the point group is 32 (or  $D_3$ ),  $\alpha$ -quartz is a dichroic compound [1]. Therefore any absorption spectrum can be expressed as a linear combination of the two spectra  $\chi_k$  and  $\chi_\perp$  corresponding to the polarisation vector  $\mathbf{e}$  of the photon beam parallel and perpendicular to the ternary axis of the hexagonal cell (i.e. the c axis), respectively. While calculations of isotropic XANES spectra of  $\alpha$ -quartz have been the subject of several studies in the past [47, 48, 49, 50, 17], little attention has been paid to the angular dependence of absorption. Lagarde et al. [51] show that the differences observed between  $\chi_k$  and  $\chi_\perp$  spectra are similar to that observed between the spectra of silica and densified silica. In Ref. [51, 52]

polarization effects are interpreted in terms of geometrical considerations. However, to our knowledge no convincing calculations of polarized data have been reported yet.

Si and O K-edge measurements were carried out respectively on the SA 32 and SA 72 beam lines at the SuperACO facility of LURE (Orsay, France). The storage ring was operating at 800 MeV ( $\gamma_c = 18.6$  Å) and 200 mA electron current. The sample was a synthetic (1010) oriented single crystal of  $\alpha$ -quartz. The SA 32 beam line was equipped with a double InSb (111) crystal monochromator. The instrumental resolution was estimated to be around 0.7 eV. The incident beam was monitored by an ionisation chamber while the absorption of the sample was measured in the electron drain current mode. Energy calibration was checked after each scan by measuring the c-Si spectrum for which the inflection point of the absorption edge was set to 1839 eV. The spectra were collected over a photon energy range of 1830–1910 eV with 0.2 eV steps and 1 s integration time. The sample was placed on a rotating holder, the rotation axis of which was parallel to the photon beam. The (1010) plane of the sample was set normal to the photon beam and the spectra were measured for the polarisation vector  $\mathbf{E}$  either parallel to the c axis ( $\parallel k$ ) or perpendicular to the c axis ( $\perp k$ ). We verified that the combination  $\frac{2}{3} \perp + \frac{1}{3} \parallel k$  reproduced the powder sample well. The X-ray natural linear dichroism (XNLD) is obtained by the difference  $\parallel k - \perp k$ . The SA 72 beam line was equipped with a toroidal grating monochromator. The estimated resolution was around 0.3 eV. Polarized O K-XANES were measured in the fluorescence mode over a photon energy range of 525–580 eV with 0.11 eV steps. The first 12 eV were slightly affected by self-absorption and the signal to noise was not good enough to permit an unambiguous extraction of the XNLD.

Calculations were performed with various sizes of cell built from the crystallographic parameters given in Ref. [53]. Convergence in terms of supercell size was obtained for a  $2 \times 2 \times 2$  supercell (72 atoms) at both silicon and oxygen K-edges. In order to show the influence of core-hole effects we also present results obtained from the primitive cell (9 atoms) with or without core-hole (ground state calculation). Charge density was calculated with  $2 \times 2 \times 2$  k-point grid for primitive cells (with or without core-hole) and only one k-point for the  $2 \times 2 \times 2$  supercell. The Lanczos basis was determined with  $4 \times 4 \times 4$  k-point grid for the primitive cell and  $3 \times 3 \times 3$  k-point grid for the supercell. The broadening parameter  $\eta$ , was set to 1 eV, this led to the construction of around 500 and 600  $\mu_i$  vectors for the primitive cell and the supercell calculations respectively.

Experimental Si K-edge X-ray absorption spectra are compared with  $2 \times 2 \times 2$  supercell calculations in figure 2. From top to bottom one can see  $\parallel k$  contribution (figure 2a),  $\perp k$  contribution (figure 2b), and the XNLD signal (figure 2c). Figure 2c shows that  $\alpha$ -quartz presents a strong angular dependence at the silicon K-edge, close to 9% of the white line's intensity. Experimental and calculated spectra { polarized and dichroic } are in excellent agreement. The strength and the energy position of all the features are correctly reproduced. At the oxygen K-edge (figures 3a and 3b) the agreement with experiment is also satisfactory.  $\parallel k$  and  $\perp k$  spectra differ essentially in the 12–19 eV energy range. These differences are well reproduced by the calculations.

Figure 4 compares three calculated  $\perp k$  spectra at both silicon and oxygen K-edges: the  $2 \times 2 \times 2$  supercell spectrum (solid line), the primitive cell calculation including core-hole effects (dashed line) and the ground state calculation (dotted line). At the silicon K-edge (upper panel), the ground state calculation does not reproduce the intense white line, which is clearly a signature of core-hole-electron interaction. Including a 1s core-hole on one of the three silicon atoms of the unit cell drastically modifies the spectrum and results in the appearance of the white line. Increasing the size of the cell yields changes that are essentially in the 8–18 eV energy range, showing that the resonances occurring in that region are related to medium range organisation around the absorbing atom. At the oxygen K-edge (lower panel), although core-hole effects are less important than at the silicon K-edge, they definitely have to be taken into account in the calculation. Furthermore our simulations show the sensitivity to medium range order of the 12–20 eV region just above the main peak.

The importance of core-hole effects in  $\alpha$ -quartz was first noticed by Jollet and Noguera [47]. This point was emphasized in multiple scattering studies [48, 50]. Our calculations confirm these previous considerations and demonstrate that reciprocal space calculations can also evidence the influence of medium range order, as is usually shown in cluster size analysis performed within the multiple scattering formalism [48, 50].

Figures 2 and 3 display a good agreement between calculated and experimental spectra. Nevertheless the agreement in energy position may be discussed to a certain extent. Indeed calculated features appear slightly too contracted compared with experiment. For example, 1 eV shift is observed at 25 eV in figure 2. This contraction becomes more pronounced as energy increases. This small discrepancy could be due to the use of DFT eigenvalues. Unfortunately, in  $\alpha$ -quartz, the GW corrections have been computed only for empty states that are close to the conduction band edge [54, 55], thus we can not verify the accuracy of a scissor-operator approximation far from the edge.

Recently Mo and Ching [17] have calculated isotropic Si and O K-XANES and the corresponding LDOS using a supercell approach within an ab initio orthogonalized linear combination of atomic

orbitals (OLCAO) method. A good agreement has been obtained between experiments and XANES calculations. With regards to LDOS calculations, the situation is quite different. They have shown that the SiK-edge can be reasonably represented by Si p LDOS, while O p LDOS surprisingly fails to reproduce any feature of the experimental spectrum. This result would mean that the radial dipole matrix element are strongly energy dependent in that case. This last consideration may be taken cautiously since the energy dependence of the dipole matrix element as well as the LDOS are widely dependent on the method used for their calculation. In particular, the LDOS depend on the size of the integration region used for the angular momentum projection. Only if this region is sufficiently small, the LDOS are independent of the size of the region, apart from a multiplicative factor. We calculated Si and O p LDOS, using an integration sphere of 0.4 Å radius. The resulting LDOS are similar to the corresponding total cross sections computed with our approach, in contradiction with the conclusions of Mo and Ching [17]. To explain this discrepancy, it should be noticed that Mo and Ching used the Mulliken population to compute the LDOS, which corresponds to a much larger effective integration region.

## 4 conclusion

We have presented an ab initio framework based on pseudopotentials for calculating XANES spectra. The scheme uses self-consistent full-potentials. It was applied to the calculation of K-edge spectra in diamond and  $\alpha$ -quartz. The results were compared with isotropic (diamond) and dichroic ( $\alpha$ -quartz) experimental data and a good agreement was obtained. In the case of diamond, our 250 atom supercell calculated spectrum is comparable with the BS calculated one of Soininen and Shirley. These first applications have shown that the introduction of the recursion method permits the treatment of large supercells. This opens new fields of applications like surfaces, small aggregates or amorphous materials, for which large supercells are required. The continued fraction may also permit the investigation of more extended x-ray absorption regions, without adding significant computation time. The results suggest that our scheme is quite robust and could be further successfully applied in XANES and ELNES spectroscopies.

We would like to thank G. Tourillon and C. Laon for having provided polarized O K-edge experimental spectra. We also thank J.J. Rehr for encouraging and fruitful discussions. The english was polished by S. Joyce. We are grateful to Ch. Bröder for his thorough reading of the manuscript. This is an IPGP contribution # XXXX.

## References

- [1] Ch. Bröder, J. Phys.: Condens. Matter 2, 701 (1990).
- [2] R. D. Cowan, The Theory of Atomic Structure and Spectra (University of California Press, Berkeley, 1981).
- [3] F. M. F. de Groot, J. Elec. Spec. 67, 529 (1994).
- [4] M. Finazzi, F. M. F. de Groot, A. Dias, B. Kierren, F. Bertran, Ph. Saintavrit, J. Kappler, O. Schulte, W. Felsch, and G. Kroll, Phys. Rev. Lett. 75, 4654 (1995).
- [5] C. R. Natoli, D. K. Misener, S. Doniach, and F. W. Kutzler, Phys. Rev. A 22, 1104 (1980).
- [6] L. Fonda, J. Phys.: Condens. Matter 4, 8269 (1992).
- [7] A. L. Ankudinov, B. Ravel, J. J. Rehr, and S. D. Conradson, Phys. Rev. B 58, 7565 (1998).
- [8] Y. Joly, Phys. Rev. B 63, 125120 (2001).
- [9] Y. Joly, D. Cabaret, H. Renvier, and C. R. Natoli, Phys. Rev. Lett. 82, 2398 (1999).
- [10] X. Weng, P. Rez, and O. F. Sankey, Phys. Rev. B 40, 5694 (1989a).
- [11] M. T. Czyzyk, R. Potze, and G. A. Sawatzky, Phys. Rev. B 46, 3729 (1992).
- [12] R. Bacończak, A. Wolska, K. Lawniczak-Jablonska, and Ph. Saintavrit, J. Phys.: Condens. Matter 12, 7371 (2000).
- [13] The transition term of the absorption cross section can be expressed as a product of an atom like term (ie., a radial matrix element), and a LDOS. This factorization is derived in appendix B of J.E. Muller and J.W. Wilkins, Phys. Rev. B, 29, 4331 (1984), and in appendix A of D.A. Muller, D.J. Singh and J. Silcox, Phys. Rev. B, 57, 8181 (1998).

- [14] P. Blaha, K. Schwarz, G. Madsen, D. Kvasnicka, and J. Luitz, *WIEN 2k, An Augmented Plane Wave + Local Orbitals Program for Calculating Crystal Properties* (Karlheinz Schwarz, Techn. Universitat Wien, Austria), 2001. ISBN 3-9501031-1-2.
- [15] M. Nehls, P. H. Louf, P. Schattschneider, P. Blaha, K. Schwarz, and B. Jourey, *Phys. Rev. B* **59**, 12807 (1999).
- [16] S. D. Mo and W. Y. Ching, *Phys. Rev. B* **62**, 7901 (2000).
- [17] S. D. Mo and W. Y. Ching, *Appl. Phys. Lett.* **78**, 3809 (2001).
- [18] Ch. J. Pickard, Ph.D. thesis, University of Cambridge (1997).
- [19] D. Jayawardane, Ch. J. Pickard, L. Brown, and M. Payne, *Phys. Rev. B* **64**, 115107:1 (2001).
- [20] K. Suenaga, E. Sandre, C. Colliex, Ch. J. Pickard, and S. Iijima, *Phys. Rev. B* **63**, 165408:1 (2001).
- [21] P. Blochl, *Phys. Rev. B* **50**, 17953 (1994).
- [22] E. L. Shirley, *Phys. Rev. Lett.* **80**, 794 (1998).
- [23] J. A. Soininen and E. L. Shirley, *Phys. Rev. B* **64**, 165112:1 (2001).
- [24] S. A. Brecht, L. Reining, R. D. Sole, and G. Onida, *Phys. Rev. Lett.* **80**, 4510 (1998).
- [25] L. X. Benedict, E. L. Shirley, and R. B. Bohn, *Phys. Rev. B* **57**, R9385 (1998a).
- [26] L. X. Benedict, E. L. Shirley, and R. B. Bohn, *Phys. Rev. Lett.* **80**, 4514 (1998b).
- [27] M. Rohlfing and S. G. Louie, *Phys. Rev. Lett.* **80**, 3320 (1998).
- [28] R. Haydock, *Solid State Physics* **35**, 215 (1980).
- [29] A natural choice for the electron partial waves is the solutions of the radial Schrodinger equation for the isolated atom.
- [30] R. Haydock, V. Heine, and M. J. Kelly, *J. Phys. C: Solid State Phys.* **5**, 2845 (1972).
- [31] R. Haydock, V. Heine, and M. J. Kelly, *J. Phys. C: Solid State Phys.* **8**, 2591 (1975).
- [32] A. Filipponi, *J. Phys.: Condens. Matter* **3**, 6489 (1991).
- [33] L. X. Benedict and E. L. Shirley, *Phys. Rev. B* **59**, 5441 (1999).
- [34] C. Lanczos, *J. Res. National Bureau. Stand.* **45**, 255 (1950).
- [35] C. Lanczos, *J. Res. National Bureau. Stand.* **49**, 33 (1952).
- [36] G. Onida, L. Reining, and A. Rubio, *Rev. Mod. Phys.* **74**, 601 (2002).
- [37] L. Hedin, *Phys. Rev.* **139**, A796 (1965).
- [38] M. S. Hybertsen and S. G. Louie, *Phys. Rev. B* **35**, 5585 (1987).
- [39] Calculations were performed with PARATEC (PARALLEL Total Energy Code) by B. Pfrommer, D. Raczkowski, A. Canning, S. G. Louie, Lawrence Berkeley National Laboratory (with contributions from F. Mauri, M. Cote, Y. Yoon, Ch. J. Pickard and P. Haynes). For more information see [www.nersc.gov/projects/paratec](http://www.nersc.gov/projects/paratec).
- [40] N. Troullier and J. L. Martins, *Phys. Rev. B* **43**, 1993 (1991).
- [41] H. J. Monkhorst and J. D. Pack, *Phys. Rev. B* **13**, 5188 (1976).
- [42] Y. Ma, N. W. Asdahl, P. Skytt, J. Guo, J. Nordgren, P. D. Johnson, J. E. Rubensson, T. Boske, W. Eberhardt, and S. D. Kevan, *Phys. Rev. Lett.* **69**, 2598 (1992).
- [43] X. Weng, P. Rez, and H. Ma, *Phys. Rev. B* **40**, 4175 (1989b).
- [44] J. J. Rehr, personal communication.
- [45] M. Rohlfing, P. Kruger, and J. Pollmann, *Phys. Rev. B* **48**, 17791 (1993).
- [46] B. A. Maud and M. A. Luani, *Phys. Rev. B* **62**, 4464 (2000).
- [47] F. Jollet and C. Noguera, *phys. stat. sol. (b)* **179**, 473 (1993).
- [48] J. Chaboy, M. Benfatto, and I. Davoli, *Phys. Rev. B* **52**, 10014 (1995).
- [49] I. Tanaka, J. Kawai, and H. Adachi, *Phys. Rev. B* **52**, 11733 (1995).
- [50] Z. Wu, F. Jollet, and F. Seifert, *J. Phys.: Condens. Matter* **10**, 8083 (1998).
- [51] P. Lagarde, A. M. F. Lank, G. Tourillon, R. C. Liebermann, and J. P. Itie, *J. Phys. I France* **2**, 1043 (1992).
- [52] F. Bart, F. Jollet, J. P. Durand, and L. Duillard, *phys. stat. sol. (b)* **176**, 163 (1993).
- [53] G. Will, M. Bellotto, W. Parrish, and M. Hart, *J. Appl. Cryst.* **21**, 182 (1988).
- [54] E. K. Chang, M. Rohlfing, and S. G. Louie, *Phys. Rev. Lett.* **85**, 2613 (2000).
- [55] V. Olevano, personal communication.



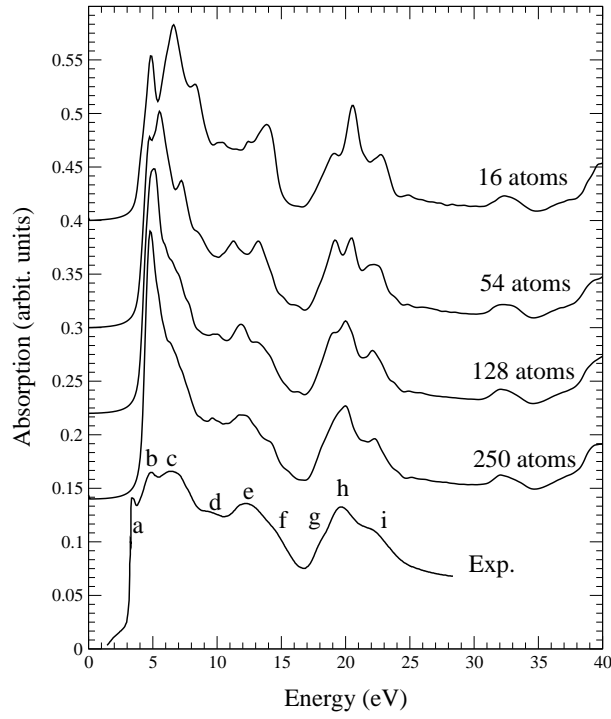


Figure 1: Calculated C K-edge X-ray absorption spectra in diamond for different supercell sizes, compared with experimental data (from Ref. [42]). A 286.1 eV shift was applied to the experimental spectrum.

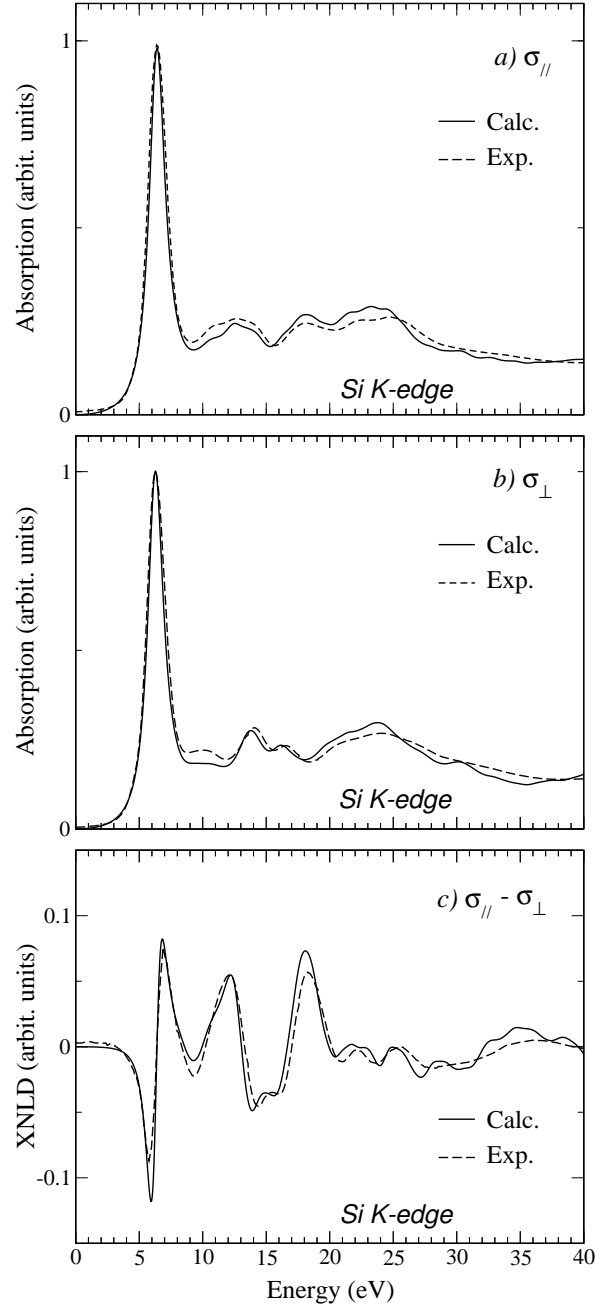


Figure 2: Experimental (dashed line) and calculated (solid line) Si K-edge polarized X-ray absorption spectra in  $\alpha$ -quartz: (a)  $\sigma_{\parallel}$  corresponding to  $k [001]$ ; (b)  $\sigma_{\perp}$  corresponding to  $k [001]$ ; (c) XNLD or  $\sigma_{\parallel} - \sigma_{\perp}$ . A 1840.7 eV shift was applied to experimental data.

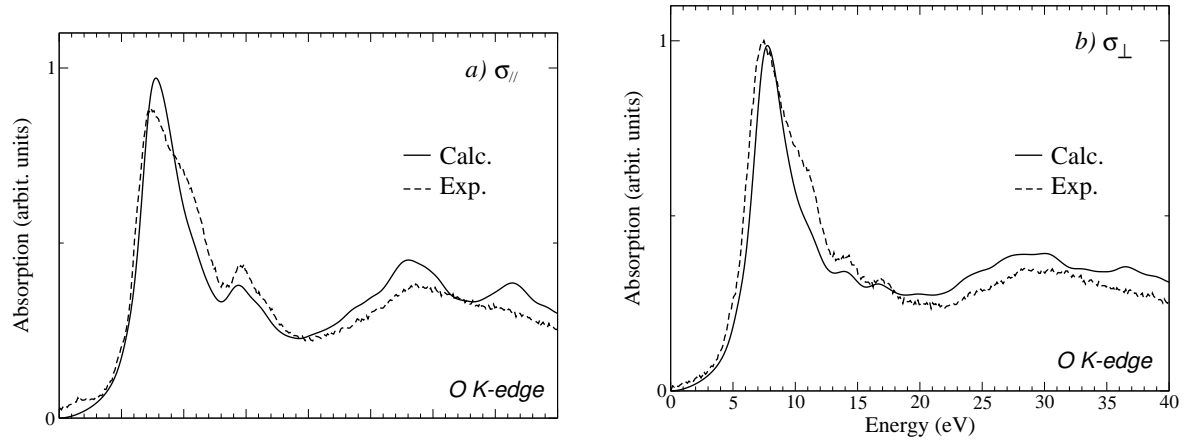


Figure 3: Experimental (dashed line) and calculated (solid line) O K-edge polarized X-ray absorption spectra in  $\alpha$ -quartz: (a)  $\sigma_{\parallel}$ ; (b)  $\sigma_{\perp}$ . A 531.9 eV shift was applied to experimental data.

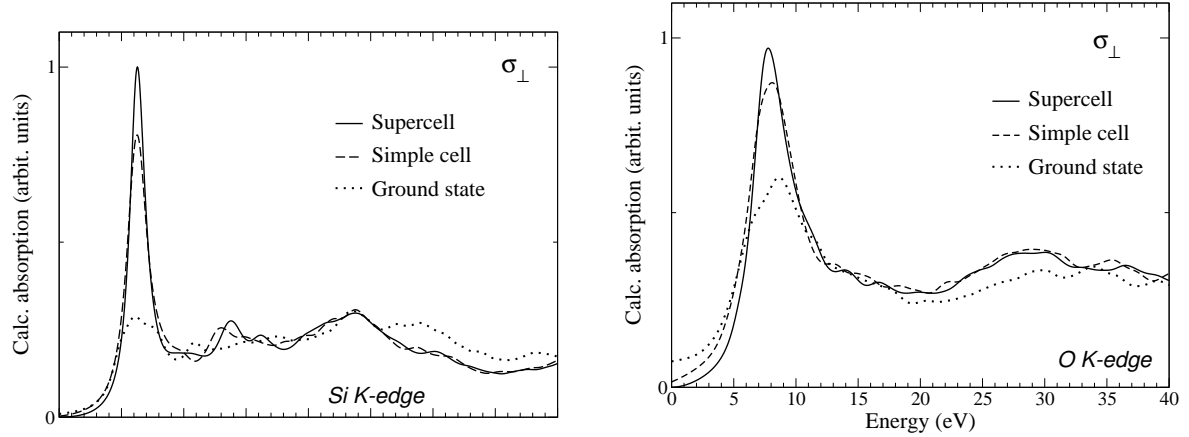


Figure 4: Calculated  $\sigma_{\perp}$  at the silicon K-edge (upper graph) and at the oxygen K-edge (lower graph) for different cells: a  $2 \times 2 \times 2$  supercell including one 1s core-hole (solid line), a simple cell (hexagonal unit cell) also including one 1s core-hole (dashed line), and the ground state hexagonal unit cell (dotted line).